Regular window structure of a double-well Duffing oscillator

V. Englisch and W. Lauterborn
Institut für Angewandte Physik, Technische Hochschule Darmstadt, Schlossgartenstrasse 7, D-6100 Darmstadt, Federal Republic of Germany
(Received 3 January 1991)

A special, seemingly infinite sequence of saddle-node bifurcations of the driven double-well Duffing oscillator is investigated. It occurs in resonances with even torsion number and shows period-adding behavior. The sequence of saddle-node bifurcations gives rise to a regular window structure of higher and higher period. An empirical law is given of the organization of periods and torsion numbers when proceeding along the sequence to the limit.

I. INTRODUCTION

The Duffing oscillator with a double-well potential is investigated. It can be described in normalized form by the three-parameter equation (1):

$$\ddot{x}+d\dot{x}-x+x^3=f\cos(\omega t)\ , \tag{1}$$

where d is the damping parameter and the further two parameters f and ω are the amplitude and the frequency of an external driving force, respectively.

The Duffing-type system, albeit looking simple with its just one nonlinear term x^3, shows a richness in behavior not yet fully explored despite many attempts [1–14]. Research along different lines has revealed the qualitative shape of its attractors and invariant manifolds [4–7] and put forward results on the coexistence of attractors [8–10] and on the bifurcation set [11–14] similar to those found for other oscillators, e.g., those described in Refs. [15–18]. A topic not yet explored in this system is the laws behind the investigated window regularities and chaotic band structure occurring repeatedly inside resonances (see, e.g., Ref. [17]). This paper presents results pertaining to a certain inner structure of chaotic bands different from what is known to occur in other systems and what is known as the Feigenbaum scenario with its inner structure [19]. It gives rise to the conjecture that a hierarchical structure within chaotic regions is observed in this system.

Written as a set of autonomous differential equations of first order, Eq. (1) has the form

$$\begin{aligned}\dot{x}_1&=x_2\ ,\\ \dot{x}_2&=-dx_2+x_1-x_1^3+f\cos(2\pi x_3)\ ,\\ \dot{x}_3&=\frac{\omega}{2\pi}\end{aligned} \tag{2}$$

with a phase space $\mathbb{R}^2\times S^1$.

Due to the symmetric potential of the Duffing system with $V(x_1)=x_1^4/4-x_1^2/2$, i.e., $V(x_1)=V(-x_1)$, Eq. (2) possesses two different kinds of closed trajectories. A periodic trajectory of this system projected onto the (x_1,x_2) plane is either inversion symmetric to itself

$$[x(t)=(x_1(t),x_2(t),x_3(t))$$
$$=(-x_1(t),-x_2(t),x_3(t)+\tfrac{1}{2})]$$

or to a coexisting asymmetric trajectory $\tilde{x}(t)\neq x(t)$ but which is inversion symmetric to

$$x(t)=(x_1(t),x_2(t),x_3(t)),$$
$$\tilde{x}(t)=(-x_1(t),-x_2(t),x_3(t)+\tfrac{1}{2})\ ,$$

as shown in Ref. [20].

Swift and Wiesenfeld [20] have shown that for systems with a symmetric vector field the Poincaré map $\mathbf{P}$: $(x,v)\rightarrow\mathbf{P}(x,v)=\Phi^T(x_1,x_2,x_3=\text{const})$ is the second iterate of a map $-\tilde{\mathbf{P}}=\mathbf{P}^{1/2}$, where $v=\dot{x}$ and T is the period of the driving ($T=1$ in our case). The orbit of $\mathbf{P}$ loses its stability and splits into two stable asymmetric orbits via a symmetry-breaking bifurcation which corresponds to the first period-doubling bifurcation of the root $\tilde{\mathbf{P}}$.

This situation is illustrated in Fig. 1 which is calculated with a damping parameter $d=0.2$. An inversion symmetric trajectory of period 1 is plotted near but just before where a symmetry-breaking bifurcation has taken place ($\omega=0.795$). Therefore the trajectory is inversion symmetric to itself [Fig. 1(a)]. After the bifurcation the orbit has lost its symmetry and the two asymmetric period-1 orbits shown in Figs. 1(b) and 1(c) coexist at $\omega=0.775$. They are inversion symmetric to each other. The basins of attraction for the Poincaré cross section $\Sigma_c=\{(x_1,x_2,c)\in[\mathbb{R}^2\times S^1\}$ with $c=0$ for the two attractors of Figs. 1(b) and 1(c) are shown in Fig. 2. The two period-1 attractors—fixed points of the Poincaré map $\mathbf{P}$—are indicated as small white squares at $(x,v)=(1.891,0.354)$ representing the orbit of Fig. 1(b) and at $(x,v)=(1.077,1.476)$ representing the corresponding inversion symmetric orbit. When applying the Poincaré map $\mathbf{P}$ with an initial condition of the grey or black area the trajectory will be attracted by the corresponding white fixed point. In addition, a third symmetric period-3 attractor coexists. Its basin is white in this figure and the periodic points are marked as black dots at $\{(x,v)\}=\{(1.434,-0.957),(-0.389,0.976),(1.892,1.481)\}$.

II. THE RECURRENT BIFURCATION STRUCTURE

Figure 3 shows a typical bifurcation diagram of Eq. (1) with the frequency ω as a bifurcation parameter. The driving amplitude is $f=10$ and the damping parameter $d=0.2$. All computations in this paper are carried out for this value of the damping. To catch coexisting solutions the diagram is calculated in the following way. For 2000 equally spaced different frequencies between

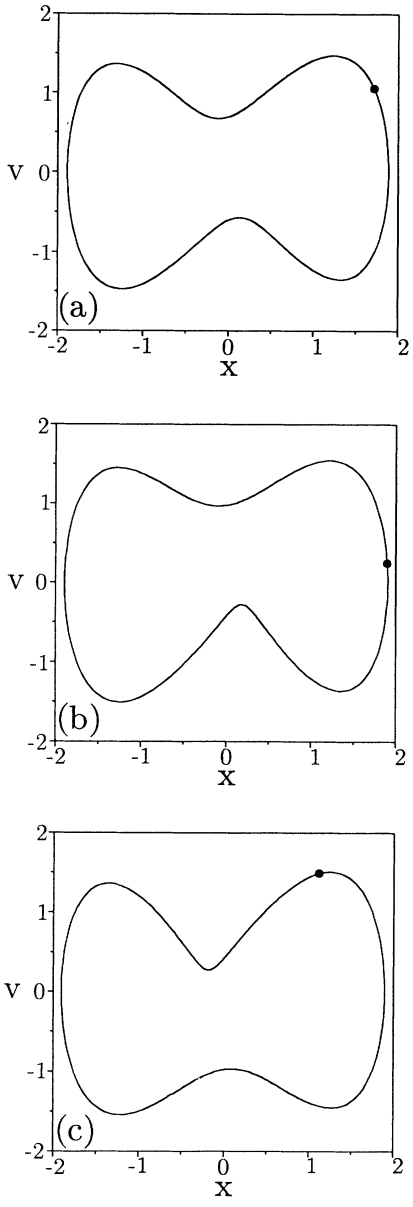

FIG. 1. A closed trajectory of a vector field with a symmetric potential $V(x_1)=V(-x_1)$ is (a) either a symmetric trajectory ($d=0.2$, $f=1$, $\omega=0.795$) or (b) and (c) one of two coexisting asymmetric trajectories which are inversion symmetric to each other ($d=0.2$, $f=1$, $\omega=0.775$). The black dots indicate the fixed points of the Poincaré map **P**.

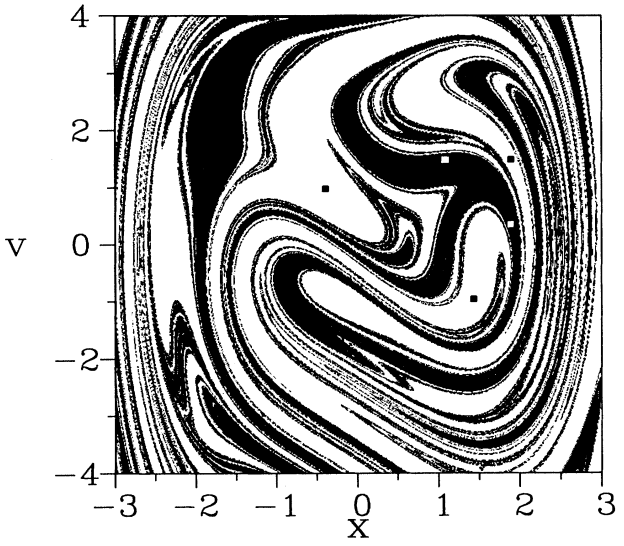

FIG. 2. The basin of attraction for the parameter values $d=0.2$, $f=1$, and $\omega=0.775$. For this parameter set there are three attractors coexisting, namely, the two asymmetric period-1 orbits shown in Figs. 1(b) and 1(c) and one symmetric period-3 orbit. The black and grey areas belong to the basin of the two period-1 orbits, whereas the white area represents the basin of attraction for the period-3 solution. The attractors are marked as black and white dots appearing in the respective areas.

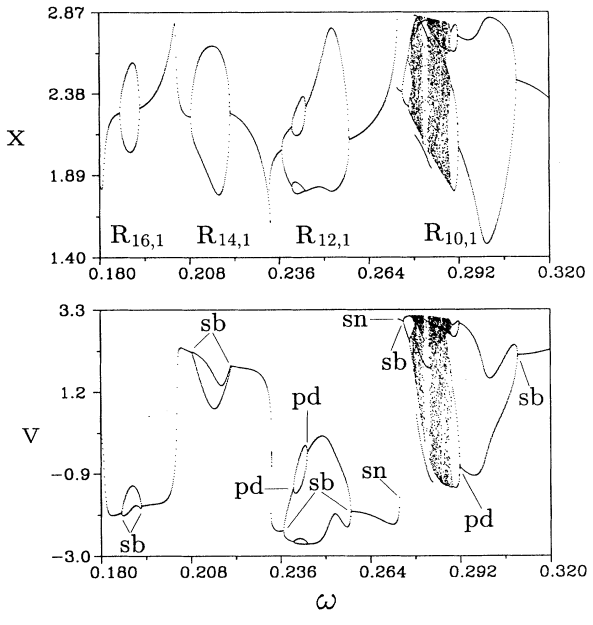

FIG. 3. Bifurcation diagram for the driving amplitude $f=10$ and the damping parameter $d=0.2$ showing the recurring structure of resonances in the parameter space. Two saddle-node (sn) bifurcations and two symmetry-breaking (sb) bifurcations alternate for the given path through the parameter space. Between the symmetry-breaking bifurcations at higher frequencies period-bubbling bifurcations occur.

$\omega=0.18$ and 0.32 Eq. (1) is solved for 32 different, equally spaced initial conditions $(\{x_0^i, v_0^i), i=1, \ldots, 32$ where $x_0^i \in]0,3[, v_0^i=0\})$. After attaining a stationary solution (the attractor), one coordinate (x and v in the upper and lower diagrams of Fig. 3, respectively) is plotted at phase $x_3=0$ of the driving for a certain number of driving cycles. Then a maximum of 32 coexisting attractors can be caught, sufficient for the present purpose. To get an overview of which and how many attractors to expect many basin calculations similar to those given in Fig. 2 have been done beforehand. When reading this type of bifurcation diagram one must be cautious as to the period of the attractors, e.g., one single period-2 attractor yields two points for one frequency value whereas two coexisting attractors, both of period 1 also yield two points for one frequency value. Thus, full information has to include trajectories for ambiguous cases.

The diagram in Fig. 3 makes visible the qualitative changes of the system in the range of the driving frequency from $\omega=0.18$ to 0.32. For the lowest driving frequency shown in this plot the response of the system is a period-1 limit cycle indicated by one dot at the corresponding ω value. This period-1 solution stays stable until the frequency reaches a bifurcation point at $\omega \approx 0.1863$ where a symmetry-breaking (sb) bifurcation takes place and two asymmetric period-1 cycles originate from the symmetric one. These two attractors coexist in the parameter region up to $\omega \approx 0.1927$ (the upper and lower branches in the diagram) where they merge again by a symmetry-breaking bifurcation. There the single symmetric period-1 attractor which became unstable resumes its stability. The region between the two symmetry-breaking bifurcation points where the symmetric period-1 orbit is unstable belongs to a resonance of the system and is labeled $R_{16,1}$ which also represents the torsion and the period at these bifurcations. In general, a resonance $R_{n,m}$ is labeled by the torsion n of the local flow around the closed unstable orbit (first index) and the period m of this orbit (second index). For the definitions see Refs. [21–23]. In the parameter region $\omega=[0.2082, 0.2210]$ the same situation as described before occurs and is labeled as the resonance $R_{14,1}$.

When the frequency is increased further, two saddle-node (sn) bifurcations occur (just visible around $\omega \approx 0.233$) comprising a region of bistability with symmetric attractors. This small region of bistability belongs to the resonance $R_{13,1}$ (not explicitly marked in the figure) that has already developed a hysteresis loop. At even higher frequencies further symmetry-breaking bifurcations take place. Additionally, it can be noticed that at the resonance $R_{12,1}$ the two asymmetric period-1 orbits double their period via a period-doubling (pd) bifurcation and then halve it by an inverse period-doubling bifurcation, so that a loop for each branch occurs. This is also called "period bubbling" [24]. For a higher driving force the parameter regions of the resonances become wider and different resonances start to overlap. Also, the corresponding period bubbling seen at the resonance $R_{12,1}$ has developed to full period-doubling cascades into chaos for the resonance $R_{10,1}$. The chaotic regions contain periodic windows which again turn into chaos via period doubling. The diagram shows the recurring structure of resonances, i.e., the alternating occurrence of saddle-node bifurcations and symmetry-breaking bifurcations, which has already been found in many other systems [14–18].

III. WINDOW STRUCTURE INSIDE A SINGLE EVEN RESONANCE

A. Observations and definitions

The parameter region of the resonance $R_{6,1}$ is chosen for a closer examination of its inner structure. We took this resonance because it is the best choice with respect to fast and efficient computation. To find the corresponding behavior in higher resonances the driving amplitude f has to be higher and/or the driving frequency ω has to be lower. Both lead to an increase in computer time. For the lower resonances ($R_{4,1}$ and $R_{2,1}$) a large number of coexisting attractors (due to the double-well potential) additionally cause an increase in computer time.

The fixed-point curves of the asymmetric period-1 solution of the resonance $R_{6,1}$ are given in Fig. 4. The fixed-point curves in this paper are calculated with a continuation program written by Knop based on standard continuation techniques and are described in detail in Refs. [15] and [25]. A fixed-point diagram is similar to a bifurcation diagram except that only one distinct periodic

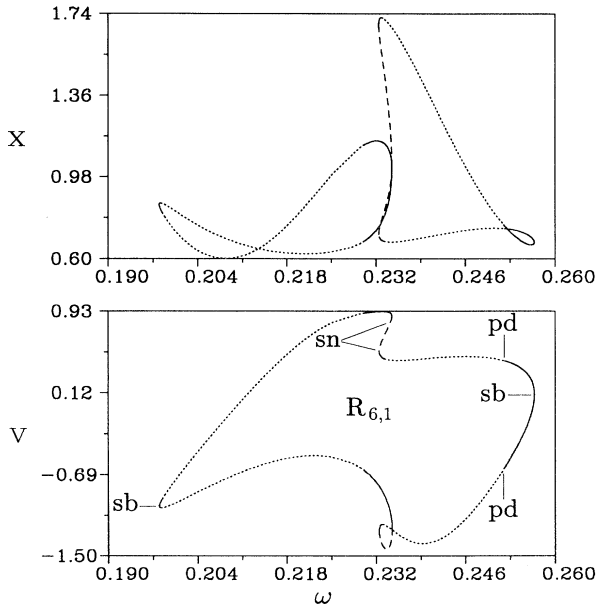

FIG. 4. A fixed-point diagram of the asymmetric period-1 solution of the resonance $R_{6,1}$ (x and v projection). The driving amplitude is $f=1$. This fixed-point curve covers the entire ω-parameter region of the resonance. The line shape indicates different states of stability (see text).

solution is followed regardless of its stability, whereas in the bifurcation diagram shown in Fig. 3 only stable solutions are shown regardless of their period. The diagram of Fig. 4 is calculated for the driving amplitude $f=1$. The stability of the solution in this plot is indicated by the line style. A solid line indicates a stable solution [the complex eigenvalues μ_i of the linearized Poincaré map $D\mathbf{P}(x,v)$ yield $|\mu_1|,|\mu_2|<1$], a dotted line indicates an unstable solution due to a period-doubling bifurcation [$\mathrm{Re}(\mu_1)$ or $\mathrm{Re}(\mu_2)<-1$] which takes over stability, and a dashed line represents an unstable solution due to a saddle-node bifurcation [$\mathrm{Re}(\mu_1)$ or $\mathrm{Re}(\mu_2)>1$]. The fixed-point curve of the period-1 solution forms a single loop and can be regarded as constituting a basic entity of the $R_{6,1}$ resonance.

The bifurcation diagram comprising a large part of the resonance $R_{6,1}$ is given in Fig. 5. This diagram has been calculated similar to that of Fig. 3. Here a set of 128 initial conditions in the range of $(x_0^i,v_0^i)=(1,0),\ldots,(3,0)$, $i=1,\ldots,128$, is used with two dots plotted for each initial condition after a suitable transient time. Again after increasing the control parameter ω by a small amount, the same set of initial conditions as before is used to calculate the final state at the parameter $\omega+\Delta\omega$. As mentioned before it is possible to detect coexisting attractors with this technique. This can be seen in the plot for the parameter $\omega\approx 0.25$, for instance, where a third attractor of period 3 exists besides the two asymmetric attractors. The three branches of the third attractor can only be seen in the upper diagram. In the lower subplot one of the branches is hidden in the chaotic region that originated from the period-1 solution. In this view of the resonance it is noticed that the chaotic regions of the resonance are interrupted by a high number of periodic windows showing certain regularities. These obvious regularities are the subject of this article and investigated in more detail below.

Several enlargements of Fig. 5 have been calculated, just one of which is shown in Fig. 6 presenting the range of $\omega=[0.205,0.220]$. The diagram is obtained in a slightly different way than the previous one. Here the x or v coordinate, respectively, of the periodic points of the Poincaré map $\mathbf{P}$ is plotted versus the control parameter ω as before. But starting with the initial condition $(x,v)=(1,0)$ at $\omega=0.205$ the Duffing equation is integrated for 100 periods of the driving frequency until the transient has died out, the trajectory is expected to be close to the attractor and the local calculation error is sufficiently small ($\epsilon\leq 10^{-6}$). Then the system is integrated for the next 150 driving periods to find out whether or not the trajectory is (low) periodic or chaotic. These 150 points (or the eventually detected m periodic points) are plotted versus the driving frequency ω. Then the param-

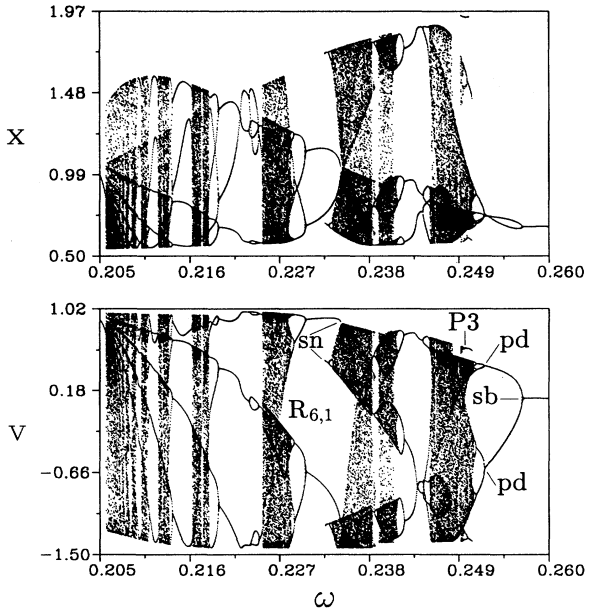

FIG. 5. Bifurcation diagram of the resonance $R_{6,1}$ for the driving amplitude $f=1$. A large number of periodic windows can be detected whereat the period of the windows seems to increase for decreasing ω value. P3 denotes a coexisting period-3 attractor.

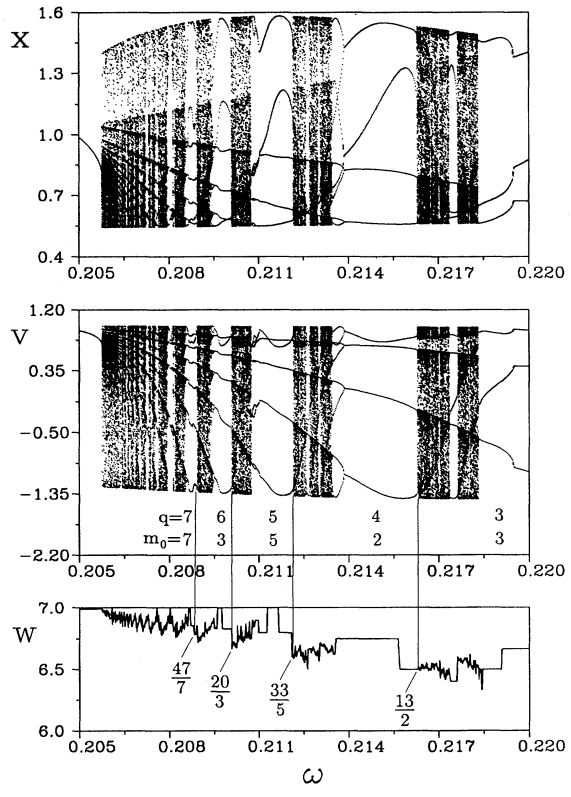

FIG. 6. Bifurcation diagram showing an enlargement of Fig. 5. For decreasing ω values the symmetry period number q is increasing by 1 for successive windows. The diagram at the bottom shows the winding number w for the parameter region shown. Here, it is increasing and converging toward $w=7$ for higher periodic windows.

eter ω is increased by a small amount ($\Delta\omega=3.33\times10^{-4}$) and integrated with an initial condition obtained from the last calculated point of the previous parameter value. Using this method of calculation one distinct attractor can be followed until it becomes unstable or until the initial point is no longer lying inside its basin of the new parameter value ω. After the parameter has reached its maximal value, it is decreased again until the starting parameter value $\omega=0.205$ is attained. When doing so there exists a possibility that a coexisting attractor is reached due to the different initial conditions which are handed over from one parameter value to the next.

Even though the structure looks similar to the bifurcation diagrams of the well-known van der Pol oscillator or other systems with a mode-locking dynamics on an invariant torus [22,26], it must be emphasized that the Duffing system investigated is a strictly dissipative oscillator. The Poincaré map is area contracting over the entire phase space with the contraction rate $\det(\boldsymbol{DP})=\exp[-(2\pi/\omega)d]<1$ which is not dependent on x_1. This means that a Hopf bifurcation cannot exist and must be excluded here. Therefore similarities with the phase-locking regions known from the van der Pol oscillator and leading to Arnold tongues cannot be expected in this system. In addition, this is not a Farey-tree ordering of the periodic windows. The period-adding ordering within a resonance found here is different but is known to appear in a wide class of systems [27]. This phenomenon has first been found in driven nonlinear series RLC circuits [27–30] showing a regular occurrence of saddle-node bifurcations forming periodic windows inside a chaotic region. For successive windows the period is increasing from m to $m+1$. The same behavior has also been modeled by piecewise linear maps [27,30], an ordinary differential equation describing the features of a driven RLC circuit [29], and a laser rate equation [17]. However, Ringland and co-workers could show in recent publications [31,32] that maps can be constructed with a transition between the Farey-tree ordering and the period adding of periodic windows.

At the right-hand side of the diagram of Fig. 6 ($\omega\leq0.22$) a period-3 window exists. This period-3 window comes into existence by a saddle-node bifurcation of a symmetric period-3 orbit such that the chaotic region (not visible on this plot) is annihilated. No hysteresis is involved here. The following bifurcation, when decreasing the parameter ω, has to break the symmetry [33] or it will be a sn bifurcation. This can be seen at $\omega\approx0.219$ where a symmetry-breaking bifurcation takes place. The next large window at lower ω seems to be a period-4 window. But in fact it is just a period-2 window as exemplified by plotting an actual orbit out of this region. Here the orbit is born asymmetrically by a saddle-node bifurcation and therefore a second asymmetric orbit—its inversion symmetric—with the same period ($m_0=2$) coexists. Both are accidentally caught—by the calculation procedure described above—one while increasing the parameter ω and the coexisting one while decreasing ω. Here the notation m_0 is used for the period where the subscript 0 denotes the "basic" period of an orbit born by an exterior saddle-note bifurcation [15]. The following bifurcation at lower ω must be a period-doubling bifurcation or a sn bifurcation. The next window at lower ω is born by a saddle-node bifurcation of a single (symmetric) orbit of period $m_0=5$. It is followed by a window of two coexisting (asymmetric) period-3 attractors and so on. So we have the case that every second "large" window is born due to a saddle-node bifurcation of a symmetric orbit with a basic period m_0, whereas every other "large" window in between consists of two coexisting orbits born as a pair by a saddle-node bifurcation. Because of this situation two new numbers p and q are introduced in the following way:

$$q=\begin{cases} m_0 & \text{for a symmetric orbit } (q\in\mathbb{N}_0 \text{ odd}) \\ 2m_0 & \text{for an asymmetric orbit } (q\in\mathbb{N}_0 \text{ even}) \end{cases}. \tag{3}$$

The number q is called the *symmetry period number,* and $\mathbb{N}_0$ is the set of non-negative natural numbers. In the same way the variable p called the *symmetry torsion number* is defined accordingly to the q value:

$$p=\begin{cases} n & \text{for } q\in\mathbb{N}_0 \text{ odd} \\ 2n & \text{for } q\in\mathbb{N}_0 \text{ even} \end{cases}, \tag{4}$$

where n is the torsion number which indicates the torsion of the local flow in units of 2π for the closed orbit (see Refs. [21], [34], and [35]). The symmetry period number q indicates the number of periodic points in the Poincaré section with the period m_0. This means q is either the number of periodic points with period m_0 in the Poincaré cross section of a single symmetric attractor or the sum of the periodic points of the asymmetric attractor with period m_0 and its counterpart. For an example refer to Fig. 5. At $\omega=0.232$ the q value is equal to 2 because the periodic window consists of two coexisting, asymmetric period-1 orbits. Their two basins are shown in Fig. 7 where the black (white) dot indicates the attractor of the Poincaré map inside the white (black) basin. The basins are calculated using about 10^5 initial conditions. Opposite this, it is $q=m_0=3$ at the parameter value $\omega=0.225$. Here a symmetric orbit is born and no other period-3 orbit exists for this parameter value. In fact there is no other attractor at all with a basin detectable within the same resolution as used in Fig. 7. So whenever q is even it means that two coexisting orbits exist with the period $m_0=q/2$.

At the bottom of Fig. 6 the (generalized) winding number [21] w is plotted. This winding number is, for the case of periodic orbits, simply related to the torsion number n and the period m of the system by

$$w=\frac{n}{m}. \tag{5}$$

Over one period of the system the torsion number n is a multiple of an integer in the vicinity of a saddle-node or symmetry-breaking bifurcation, because here the two complex eigenvalues of the linearized Poincaré map become real and one of them crosses the unit circle of the complex plane at $+1$. For a period-1 orbit Eq. (5) implies that the torsion number and winding number are the same as long as the eigenvalues are real. Near a

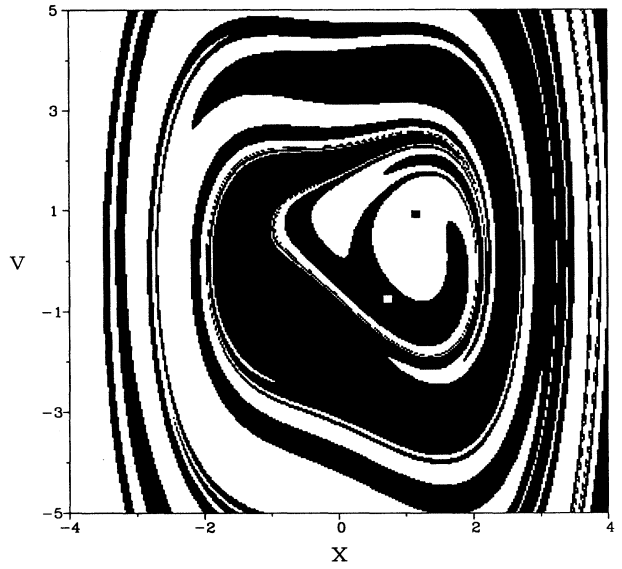

FIG. 7. The basins of the two asymmetric period-1 orbits are shown for the parameter values $f=1$ and $\omega=0.232$. The attractors are marked as a white or black square at $(x,v)=(0.7279,-0.7585)$ (white) and $(x,v)=(1.1496,0.9227)$ (black).

period-doubling bifurcation the torsion number is a constant multiple of $\frac{1}{2}$ when related to the bifurcating orbit with the lower period while one eigenvalue of the linearized Poincaré map $D\mathbf{P}$ of the doubling orbit crosses the unit circle of the complex plane at -1. This means that near a saddle-node, symmetry-breaking and period-doubling bifurcation the winding number is constant in a certain parameter region around a bifurcation point and it forms (possibly very small) plateaus when plotted versus one of the parameters of Eq. (1). Figure 6 (bottom) shows the evolution of the winding numbers for the bifurcation diagram above. For a further discussion of winding numbers and their properties see Ref. [21].

B. Formulation of a law for the winding number sequences

The winding numbers of the parameter values for which a saddle-node bifurcation occurs are noted. When decreasing the ω values from 0.225 to the beginning of the region shown, the winding numbers lead to the following sequence for successive windows (cf. Fig. 6):

$$w=\frac{n}{m_0}:\ \frac{19}{3}\ \underset{+2}{\overset{+14}{\rightarrow}}\ \frac{13}{2}\ \underset{+1}{\overset{+7}{\rightarrow}}\ \frac{33}{5}\ \underset{+2}{\overset{+14}{\rightarrow}}\ \frac{20}{3}\ \underset{+1}{\overset{+7}{\rightarrow}}\ \frac{47}{7}\ \underset{+2}{\overset{+14}{\rightarrow}}\ \frac{27}{4}\ \underset{+1}{\overset{+7}{\rightarrow}}\ \cdots \quad . \tag{6}$$

This scheme shows two interwined subsequences. One of them—valid for the windows developed by the saddle-node bifurcation of symmetric orbits—increases the torsion number n by 14 at every step to the next element of the sequence and increases the period m_0 by 2. For the other subsequence, the torsion number is increased by 7 and the period by 1 which is valid for the windows consisting of two asymmetric orbits. To put this into account the sequence of winding numbers given above can be rewritten in terms of p and q without changing the value of the winding numbers and the modified complete sequence of fractions is obtained:

$$w=\frac{p}{q}:\ \frac{19}{3}\ \underset{+1}{\overset{+7}{\rightarrow}}\ \frac{26}{4}\ \underset{+1}{\overset{+7}{\rightarrow}}\ \frac{33}{5}\ \underset{+1}{\overset{+7}{\rightarrow}}\ \frac{40}{6}\ \underset{+1}{\overset{+7}{\rightarrow}}\ \frac{47}{7}\ \underset{+1}{\overset{+7}{\rightarrow}}\ \frac{54}{8}\ \underset{+1}{\overset{+7}{\rightarrow}}\ \cdots \quad . \tag{7}$$

Obviously the sequence follows a certain rule where the p values increase by 7 when moving from one to the next window whereas the q values increase by 1. This is rewritten as a recursive formula in the following way:

$$\begin{aligned} &p_1=5,\quad q_1=1\ , \\ &w_1=\frac{p_1}{q_1}=\frac{5}{1}\ , \\ &w_{k+1}=\frac{p_{k+1}}{q_{k+1}}=\frac{p_k+7}{q_k+1}\ , \end{aligned} \tag{8}$$

where p_k is the symmetry torsion number at the "birth" of the period-q_k orbit. This formulation can be made explicit because of its simplicity:

$$w_k=\frac{p_k}{q_k}=\frac{p_1+7(k-1)}{q_1 k}=\frac{5+7(k-1)}{k},\quad k=1,2,3,\ldots\ . \tag{9}$$

The cases $k=1$ and $k=2$ are added to complete the recursive formulation. The corresponding "windows" of periodic solutions are special cases but naturally fit into the series. This becomes clear when the limits of the resonance $R_{6,1}$ to the neighboring resonances $R_{5,1}$ and $R_{7,1}$ are considered. The sequence starts with the winding number $w_1=\frac{5}{1}$ which belongs to the former saddle-node bifurcation of the period-1 solution in the neighboring resonance $R_{5,1}$. The end of the sequence is obtained as the limiting value of w_k for $k\rightarrow\infty$:

$$w_\infty=\lim_{k\rightarrow\infty} w_k=\lim_{k\rightarrow\infty}\frac{p_k}{q_k}=\lim_{k\rightarrow\infty}\frac{p_1+7(k-1)}{k}=7\ . \tag{10}$$

The winding number limit $w_\infty=7$ is the $w_1(=p_1)$ value of the next saddle-node bifurcation of the period-1 solution as can already be guessed when looking at the plot of winding numbers in Fig. 6.

The case $k=2$ leads to $w_2=\frac{12}{2}$ and corresponds to two asymmetric period-1 solutions of torsion number 6 which

developed at the sb point. Thus a complete window cascade exists covering the range of winding numbers from 5 to 7. It has been found numerically by the authors that similar cascades exist between every two odd winding numbers with period number 1, so that Eq. (9) can be written in a more general form:

$$w_k = \frac{p_1 + (p_1+2)(k-1)}{k}, \quad k = 1,2,3,\ldots . \tag{11}$$

Using l as a label for the sequences according to the resonance wherein they can be found it then reads for even winding numbers $w = n$

$$\begin{aligned} &p_1^l = l-1\ , \quad q_1^l = 1\ , \quad l = 2,4,6,\ldots \\ &w_k^l = \frac{p_k^l}{q_k^l} = \frac{(l-1)+(l+1)(k-1)}{k} \quad k = 1,2,3,\ldots \end{aligned} \tag{12}$$

with the limit

$$w_\infty^l = \lim_{k\to\infty} w_k^l = l+1\ . \tag{13}$$

It is well known that, in the case of a fully developed saddle-node sequence, the period of the windows, when coming from high ω values to lower ones, increases to infinity [36–38]. The parameter values of the saddle-node bifurcations for which the winding number sequence is valid accumulate at the parameter $\omega_{\min}^l = \omega_\downarrow(w_\infty^l)$ where the corresponding sequence limit w_∞^l is reached. Here the arrow subscript denotes the decrease of the parameter ω. With increasing period the width of the windows, i.e., the parameter regions where the saddle-node bifurcation of a period m_0 occurs and stays stable until the period-doubling cascade sets in are getting smaller. Due to the period-bubbling phenomenon the sequence limit w_∞^l [Eq. (13)] is reached at two different parameter values for the resonance $R_{n=l,1}$ (compare Figs. 10 and 11 below). When increasing the parameter ω there also exists an upper bound $\omega_{\max}^l$ of successive ω values for which a saddle-node bifurcation with increasing period occurs such that $\omega_{\max}^l = \omega_\uparrow(w_\infty^l)$.

C. Membership questions

From the bifurcation diagram Fig. 6 many more (smaller) windows can be detected, e.g., the period-5 window at $\omega \approx 0.2175$ inside the chaotic region which lies between the large windows with symmetry period numbers 3 and 4. These periods have different properties than those extracted for the above sequence. To show this, fixed-point curves of the first few periodic windows are calculated for the $l = 6$ sequence. In a fixed-point diagram a period-m orbit is represented by m separated coexisting loops, according to their m periodic points because, when taking the m-fold iterate $\mathbf{P}^m$ of the Poincaré map $\mathbf{P}$, this corresponds to m different fixed points. The fixed-point loops for the windows with $q = i$, $i = 3,\ldots,8$ are given altogether in one plot (Fig. 8). The solid lines which mark the stable solutions are the same that appear in the bifurcation diagram of Fig. 5. The unstable branches extend to lower frequencies far below the ω value of the sequence investigated with the limit $\omega_{\min}^6$. The small additional loops for $q = 3$ at the high-frequency end are added for completeness (symmetry broken period-3 solution). It can be seen clearly, that a certain

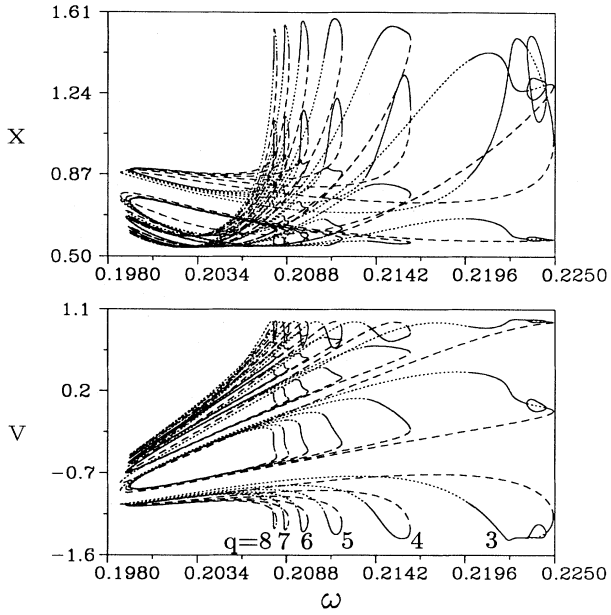

FIG. 8. All fixed-point curves for the periodic windows with the symmetry period numbers $q = i$, $i = 3,\ldots,8$. The loops are frequency interlocked. Different line shapes indicate different states of stability as in Fig. 4.

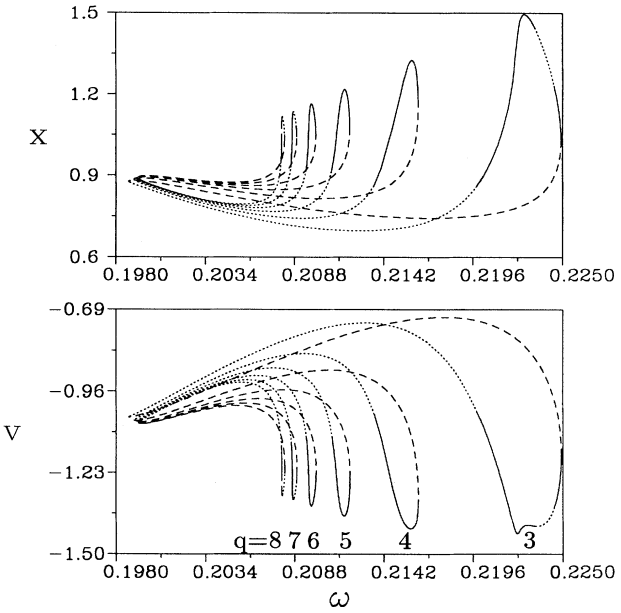

FIG. 9. One loop of each window shown in Fig. 8 is displayed to emphasize the ordering of the fixed-point curves in the parameter space. An ordering of the loops from the right to the left for higher q values can clearly be seen.

organization of the loops exist. The shape of the loops is similar for different q, and they are grouped in a regular way. For better visualization just one sequence of loops is extracted from Fig. 8—similar to the subharmonic bifurcation diagram introduced in Ref. [26]—and shown enlarged in Fig. 9. Exactly one of the q loops of each window calculated is shown. It can be seen that the qualitative shape of corresponding loops for each window is the same although every second one belongs to one of the two coexisting asymmetric attractors. The phase curves are different (symmetric or asymmetric) but the fixed point curves are not. In addition, the loops are frequency interlocked. The ω-parameter interval, where a period-$(q+1)$ orbit exists, is always a subset of the interval of the q window, $\forall q \in \mathbb{N}$: $[\omega_{q+1,\min};\omega_{q+1,\max}] \subset [\omega_{q,\min};\omega_{q,\max}]$, which can be seen from Figs. 9 and 10. The latter is an enlargement of the left tip of the fixed-point curves from Fig. 9. The maximum of the ω values for increasing period is converging to the left towards the limit $\omega^6_{\min}$ (Fig. 9), as already mentioned above, whereas the minimum of the ω values for these periods is converging to the right [37,38] as shown in Fig. 10. Therefore the parameter range where a periodic window with a high period exists is getting smaller [36]. At the maximum and minimum parameters $\omega^6_{\min}$ and $\omega^6_{\max}$ for all integers an unstable orbit with this period exists.

The following fixed-point diagrams introduce fixed-point curves of two periodic windows which are not members of the investigated ($l=6$) sequence, namely, the windows with the symmetry period numbers $q_s=6$ and

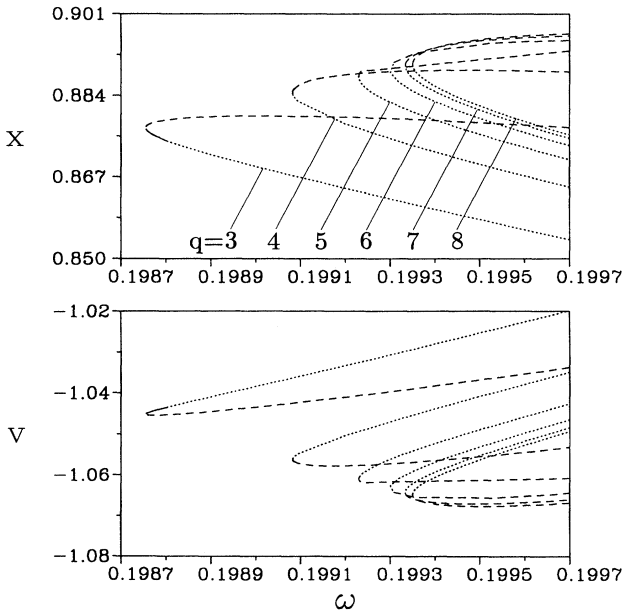

FIG. 10. An enlargement of the left part of Fig. 9 showing the ordering at the low-frequency end of the loops from left to right for windows with higher symmetry period number q.

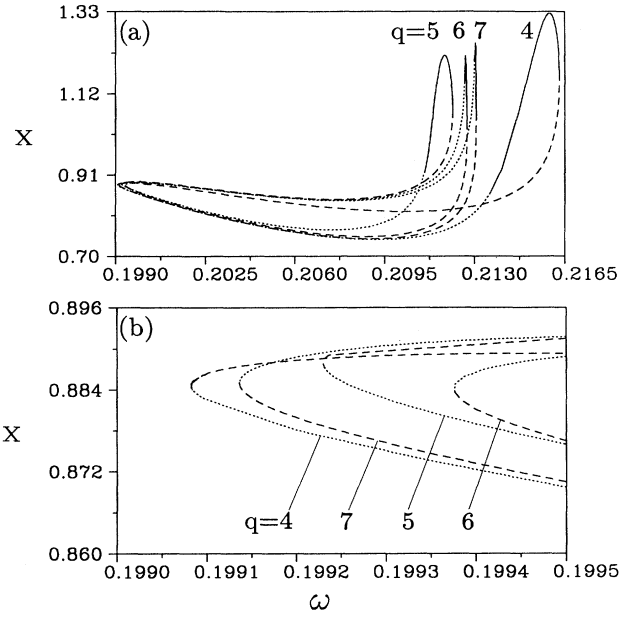

FIG. 11. (a) The fixed-point loops of the main windows with symmetry period numbers $q=5$ and $q=4$ and the surplus windows with $q=6$ and $q=7$ within the chaotic region between their stable high-frequency solutions. (b) Enlargement of (a) for the low-frequency range of the fixed-point loops. The parameter range for the subwindows is not limited by the main-window fixed-point loops.

$q_s=7$ within the chaotic region between the windows $q=5$ and $q=4$ (Fig. 11, cf. Fig. 6). [Note that there are $q-3$ windows, when the larger of the two q values is taken, and their symmetry period number q_s lies in the range from $q_s=q+1,\ldots,2(q-1)-1$.] These windows are called subwindows and subscripted with an s to distinguish them from the windows belonging to the "main" period-adding sequence. The fixed-point curves of the subwindows seem to match the gross appearance of the fixed-point curves of the large main windows but the parameter range of their existency is not limited by the main windows as can be seen from the magnification [Fig. 11(b)] of the left border of the four fixed-point loops from Fig. 11(a). Here the fixed-point curve of the $q_s=6$ window is not bordered by the loops of the $q_s=7$ and $q=5$ window as is the case for high frequencies [Fig. 11(a)]. However, it is conjectured that the saddle-node bifurcations and the fixed-point curves of the subwindows also produce sequences so that it might be possible to find a complete hierarchy of periodic windows and their winding number sequences within resonances. A closer examination of the subwindows will be given elsewhere.

IV. CONCLUSION

A special, infinite sequence of saddle-node bifurcations giving rise to a regular window structure is found in the double-well Duffing system. The sequence is made up by two subsequences of increasing periods. Such a sequence

belongs to every resonance with even torsion number and is a dominant part of the inner structure of the bifurcation set of a resonance. Fixed-point diagrams are of great help in locating those sequences because they form a loop structure and give hints for grouping windows as belonging together. The limits, specific ω values for a specific resonance and parameter set, are points where the complexity and strong dependence of the solution on ω suddenly drops back to simplicity, a simple period-1 solution, for instance. The same situation has been found in a simple sinusoidal driven laser oscillator [17] and is expected to belong also to the universal bifurcation structure of a certain class of oscillators with symmetric potential [39].

It can be expected that the surplus windows not investigated in the present paper also form series, presumably with a more complex law than the one given here. These investigations show how complicated the behavior of the simple driven Duffing oscillator is and that there is yet a long way before the complete bifurcation structure can be stated even in a qualitative, topological way.

ACKNOWLEDGMENTS

We would like to thank U. Parlitz and C. Scheffczyk for many helpful discussions as well as W. Knop and M. Wiesenfeldt for improving the readability of the manuscript. We thank the Nonlinear Dynamics group of the Institut für Angewandte Physik, Technical University Darmstadt for their constant support. In addition we would like to thank W. Knop for entrusting to us his computer code for the calculation of the fixed-point curves and F. Knocke for shading Fig. 2. This work was supported by the Stiftung Volkswagenwerk and the Sonderforschungsbereich Nichtlineare Physik (SFB 185). The computations have been done on the CRAY-XMP at the Konrad-Zuse-Zentrum für Informationstechnik Berlin, the CRAY-YMP at the KFA Jülich, the IBM 3090/200 of the Gesellschaft für Wissenschaftliche Datenverarbeitung at Göttingen, the VAX 8530 of the Technical University Darmstadt, and the SUN-System, including the Mercury Array processor MC 6400, of the Institut für Angewandte Physik, Darmstadt.

[1] G. Duffing, *Erzwungene Schwingungen bei Veränderlicher Eigenfrequenz und ihre Technische Bedeutung* (Vieweg, Braunschweig, 1918), in German.
[2] P. Holmes, Philos. Trans. R. Soc. London Ser. A **292**, 419 (1979).
[3] W. S. Loud, Duke Math. J. **24**, 63 (1957).
[4] F. C. Moon and G. -X. Li, Physica D **17**, 99 (1985).
[5] P. Holmes and D. Whitley, Physica D **7**, 111 (1983).
[6] Y. H. Kao, J. C. Huang, and Y. S. Gou, Phys. Rev. A **35**, 5228 (1987).
[7] Y. Ueda, J. Stat. Phys. **20**, 181 (1979).
[8] F. C. Moon and G.-X. Li, Phys. Rev. Lett. **55**, 1439 (1985).
[9] F. T. Arecchi, R. Badii, and A. Politi, Phys. Rev. A **32**, 402 (1985).
[10] C. Pezeski and E. H. Dowell, Physica D **32**, 194 (1988).
[11] C. Holmes and P. Holmes, J. Sound Vib. **78**, 161 (1981).
[12] H. Kawakami, IEEE Trans. Circuits Syst. **31**, 248 (1984).
[13] J. M. T. Thompson, Proc. R. Soc. London, Ser. A **421**, 195 (1989).
[14] U. Parlitz and W. Lauterborn, Phys. Lett. A **107**, 351 (1985).
[15] W. Knop and W. Lauterborn, J. Chem. Phys. **93**, 3950 (1990).
[16] T. Kurz and W. Lauterborn, Phys. Rev. A **37**, 1029 (1988).
[17] W. Lauterborn and R. Steinhoff, J. Opt. Soc. Am. B **5**, 1097 (1988).
[18] U. Parlitz, V. Englisch, C. Scheffczyk, and W. Lauterborn, J. Acoust. Soc. Am. **88**, 1061 (1990).
[19] P. Coullet and J. P. Eckmann, *Iterated Maps on the Interval as Dynamical Systems* (Birkhäuser, Boston, 1980).
[20] J. W. Swift and K. Wiesenfeld, Phys. Rev. Lett. **52**, 705 (1984).
[21] U. Parlitz and W. Lauterborn, Z. Naturforsch. A **41**, 605 (1986).
[22] U. Parlitz and W. Lauterborn, Phys. Rev. A **36**, 1428 (1987).
[23] W. Lauterborn and U. Parlitz, J. Acoust. Soc. Am. **84**, 1975 (1988).
[24] M. Bier and T. C. Bountis, Phys. Lett. A **104**, 239 (1984).
[25] R. Seydel, *From Equilibrium to Chaos* (Elsevier, New York, 1988).
[26] W. Lauterborn and I. Eick, J. Opt. Soc. Am. B **5**, 1084 (1988).
[27] J. M. Perez, Phys. Rev. A **32**, 2513 (1985).
[28] W. Meyer-Ilse, Ph.D. thesis, Göttingen University, 1984, in German.
[29] S. D. Brorson, D. Dewey, and P. S. Linsay, Phys. Rev. A **28**, 1201 (1983).
[30] S. Tanaka, T. Matsumoto, and L. O. Chua, Physica D **28**, 317 (1987).
[31] J. Ringland and M. Schell, Phys. Lett. A **136**, 379 (1989).
[32] J. Ringland, N. Issa, and M. Schell, Phys. Rev. A **41**, 4223 (1990).
[33] R. Räty, J. von Boehm, and H. M. Isomäki, Phys. Lett. A **103**, 289 (1984).
[34] P. Beiersdorfer, J. M. Wersinger, and Y. Treve, Phys. Lett. A **96**, 269 (1983).
[35] P. Beiersdorfer, Phys. Lett. A **100**, 379 (1984).
[36] P. Gaspard and X.-J. Wang, J. Stat. Phys. **48**, 151 (1987).
[37] J. Guckenheimer and P. Holmes, *Nonlinear Oscillations, Dynamical Systems and Bifurcations of Vector Fields* (Springer, Berlin, 1983).
[38] N. K. Gavrilov and L. P. Shilnikov, Math. USSR Sb **88**, 467 (1972); **90**, 239 (1973).
[39] C. Scheffczyk, U. Parlitz, T. Kurz, W. Knop, and W. Lauterborn, Phys. Rev. A **43**, 6495 (1991).